Available online at www.sciencedirect.com
ScienceDirect
C. R. Physique 9 (2008) 142–152
COMPTES RENDUS PHYSIQUE
http://france.elsevier.com/direct/COMREN/

Recent developments in terahertz optoelectronics/Développements récents en optoélectronique térahertz

Ion-irradiated $In_{0.53}Ga_{0.47}As$ photoconductive antennas for THz generation and detection at 1.55 μm wavelength

Juliette Mangeney *, Paul Crozat

Institut d'électronique fondamentale, CNRS UMR 8622, Université Paris sud, 91405 Orsay cedex, France

Available online 31 October 2007

Abstract

We present a detailed study of the photoconductive antennas made from heavy-ion-irradiated $In_{0.53}Ga_{0.47}As$ material. The optical and transport properties of ion-irradiated $In_{0.53}Ga_{0.47}As$ material are characterized. The terahertz waveforms emitted and detected by ion-irradiated $In_{0.53}Ga_{0.47}As$ photoconductive antennas excited by 1.55 μm wavelength femtosecond laser pulses are reported and the effect of the carrier lifetime on the terahertz signal characteristics emitted by such devices is analysed. The performances of ion-irradiated $In_{0.53}Ga_{0.47}As$ photoconductive antennas excited by 1.55 μm and also by 0.8 μm wavelength femtosecond laser pulses are compared to those of similar low-temperature-grown GaAs photoconductive antennas. ***To cite this article: J. Mangeney, P. Crozat, C. R. Physique 9 (2008).***

Résumé

Génération et détection de rayonnement térahertz à l'aide d'antennes photo-conductricives, en $In_{0,53}Ga_{0,47}As$ bombardé ioniquement, excitées par des impulsions laser femtosecondes de 1,55 μm de longueur d'onde. Nous décrivons une étude détaillée d'antennes photo-conductricives réalisées à partir de $In_{0,53}Ga_{0,47}As$ préalablement bombardé par des ions lourds. Les propriétés optiques et électriques de ce matériau sont caractérisées. Nous présentons les signaux impulsionnels THz émis et détectés par ces antennes, excitées par des impulsions laser femtosecondes de 1,55 μm de longueur d'onde. Nous analysons en particulier l'effet de la durée de vie des porteurs photogénérés sur les caractéristiques du signal THz émis. Nous avons aussi étudié les performances de ces antennes lorsqu'elles sont excitées par des impulsions laser femtosecondes de 0,8 μm de longueur d'onde et nous avons comparé ces performances à celles d'antennes similaires fabriquées avec du GaAs épitaxié à basse température. ***Pour citer cet article : J. Mangeney, P. Crozat, C. R. Physique 9 (2008).***

Keywords: Terahertz; Photoconductive antenna; Femtosecond optical pulse; Telecommunication wavelength; Ionic irradiation

Mots-clés : Térahertz ; Antenne photo-conductive ; Impulsion laser femtoseconde ; Longueur d'onde pour la télécommunication ; Radiation ionique

* Corresponding author.
E-mail address: juliette.mangeney@ief.u-psud.fr (J. Mangeney).

1631-0705/$ – see front matter
doi:10.1016/j.crhy.2007.07.008

1. Introduction

The terahertz frequency region of the electromagnetic spectrum has been for a long time a poorly mastered frequency range as techniques commonly used in the well-established neighboring bands are not adapted. Motivated by applications ranging from fundamental studies of collective processes in condensed matter to medical imaging, advanced material research has provided in the past 20 years new sources and detectors. Among them, photoconductive antennas excited by femtosecond laser pulses are mostly used to generate and detect broadband terahertz radiation. The best terahertz performances are achieved by photoconductive antennas made from annealed low-temperature-grown GaAs (LTG) material, since this material associates both subpicosecond carrier lifetime and high dark resistivity [1]. These devices are excited by femtosecond optical pulses with ∼800 nm center wavelength delivered by mode-locked Ti:sapphire laser. The capability of these ultrafast photoconductive antennas to generate [2] and detect [3] terahertz radiation in the frequency range from 0.3 to over 30 THz have made them extremely useful as source and detector for ultrabroadband terahertz spectroscopy systems [4] The use of ultrafast materials with smaller band gap, such as $In_{0.53}Ga_{0.47}As$, would enable cheaper more compact and turnkey terahertz spectroscopy setups based on Erbium fiber lasers which can produce femtosecond pulses at a central wavelength of 1.55 μm. Combining a compact system of this type with communications wavelength optical fibres opens the way for the generation and the detection of terahertz pulses in small, extreme, or otherwise inaccessible environments (e.g. in an endoscope or in the cavity of a pulsed magnet). Moreover, because the bandgap of the $In_{0.53}Ga_{0.47}As$ is smaller than that of GaAs, $In_{0.53}Ga_{0.47}As$ semiconductor shows a higher electron mobility which may results in an improvement of the radiated power by photoconductive antennas made from $In_{0.53}Ga_{0.47}As$ material [5].

2. State of art in 1550 nm ultrafast $In_{0.53}Ga_{0.47}As$ photoconductive antennas

In annealed LTG GaAs material, the ultra-short carrier lifetimes combined with the semi-insulating characteristics are attributed to the existence of defects related to As antisites. These defects, commonly named EL-2 like defects, add a deep level band in the gap that pins the Fermi level near the middle of the gap. A challenge is then to obtain similar characteristics in $In_{0.53}Ga_{0.47}As$ lattice matched to InP material because of its large absorption at the 1300–1550 nm wavelengths. $In_{0.53}Ga_{0.47}As$ is, however, much more challenging for ultrafast applications than GaAs because the smaller band gap tends to make the electrical resistivity extremely low at room temperature.

Low-temperature growth of $In_{0.53}Ga_{0.47}As$ was attempted early on and led to the achievement of picosecond carrier lifetime [6] However, the As antisites in $In_{0.53}Ga_{0.47}As$ create shallow donors and, together with other intrinsic defects prevents fabrication of highly resistive layers [7]. Be doping has been reported to increase the dark resistivity to ∼200 Ω cm and to reduce the carrier lifetime down to picosecond values in low-temperature-grown $In_{0.53}Ga_{0.47}As$ [8] through the compensation of donor states formed by the antisite As and the suppression of As precipitate formation. Recently, Takazato et al. have reported terahertz wave detection using Be-doped low-temperature-grown $In_{0.53}Ga_{0.47}As$ photoconductive antennas excited by femtosecond optical pulses at 1560 nm wavelength [9]. The spectral range of the detected radiation exceeds 3 THz, with a dynamic range of about 55 dB below 1 THz.

As alternatives, the incorporation of ErAs particles in $In_{0.53}Ga_{0.47}As$ alloys have been investigated by D. C. Driscoll et al. [10] Metal particles of ErAs act as fast carrier recombination centers and provide picosecond carrier lifetime. However, the growth of ErAs: $In_{0.53}Ga_{0.47}As$ structures produces undesirable low-resistivity, n-type material. The continuous density of states in the semi-metallic ErAs particles allows the Fermi level to be tuned toward midgap by compensating the free-electron concentration with discrete Be acceptor levels. Moreover, carrier lifetime can be further reduced by doping with Be, as positively charged deep levels are created along with negatively charged Be shallow-level acceptors. Thereby, optimized Be-doped ErAs: $In_{0.53}Ga_{0.47}As$ structures that associate carrier lifetime as short as 0.3 ps with dark resistivity of 500 Ω cm have been achieved [11] Be-doped ErAs: $In_{0.53}Ga_{0.47}As$ materials, which have been successfully integrated in photomixers for the generation of continuous terahertz waves [12], is nevertheless very promising for the development of broadband terahertz photoconductive antennas triggered with 1550 nm wavelength femtosecond optical pulses.

Ultrafast carrier lifetimes have also been achieved in $In_{0.53}Ga_{0.47}As$ through Fe implantation. In Fe-implanted $In_{0.53}Ga_{0.47}As$ material, defects have two sources: complexes resulting from Fe incorporation and isolated native defects caused by disorder within the lattice itself. The native defects are presumably donor levels with activation energy of 30–40 meV leading to low dark resistivity. In return, incorporation of Fe atoms in cation sites results in a

deep acceptor with an energy level of ∼0.35 eV which shifts the Fermi level towards the midgap and thus increases the dark resistivity. Thus, Fe implantation in $In_{0.53}Ga_{0.47}As$ material provides carrier lifetime of 0.3 ps and dark resistivity of hundreds Ω cm [13]. Suzuki et al. have developed photoconductive antennas made from Fe-implanted $In_{0.53}Ga_{0.47}As$ material and have reported terahertz emission [14] and detection [15] up to 2 THz from these devices excited by femtosecond optical pulses of 1.56 μm wavelength.

Finally, heavy-ion irradiation is another technique of choice to make $In_{0.53}Ga_{0.47}As$ alloys that combine subpicosecond lifetimes and good transport characteristics. This approach mainly differs from the previous ones by the fact that no impurity is introduced in the $In_{0.53}Ga_{0.47}As$ material: defects are only native defects resulting from the rupture of the crystal lattice periodicity. In this article, we present a detailed study of photoconductive antennas based on ion-irradiated $In_{0.53}Ga_{0.47}As$ material as well as the applicability of these photoconductive antennas to generate and detect broadband terahertz radiation.

3. Heavy-ion-irradiated $In_{0.53}Ga_{0.47}As$ material

The ion irradiation technique consists in bombardment of materials with ions. Contrary to the implantation, during the irradiation process, the ions used for bombardment have enough energy to go completely through the active layer and thus are no longer present in the target material. During their traveling, the incident ions enter in collision with host atoms, and from nuclear collisions, give to host atoms a part of their energy. The host atoms can then move along the crystal and eventually, themselves, enter in collision with other host atoms, thus creating a cascade of secondary displacements. These host atom displacements are as important as displacement of native defects. Due to the high transferred energy between incident ions with heavy mass and host atoms, the heavy-ion irradiation technique creates a majority of defect clusters [16]. The distinctive feature of the ion irradiation process is that only native defects are created and hardly any impurity is added in the material. The comparison of experiments performed on $In_{0.53}Ga_{0.47}As$ layers (transmission electron microscopy, pump-probe experiments versus temperature, Hall measurements and photocurrent spectroscopy) with models (thermal diffusion of defects and scattering of free carriers on defects) has given information on the nature of the defects created by heavy-ion irradiation.

Heavy ion-irradiation process (Br^+, Au^+) creates in majority defect clusters and some few point defects [17]. Fig. 1 shows the 002 dark field image of an $In_{0.53}Ga_{0.47}As$ layer irradiated with a 1×10^{12} cm^{-2} Au^+ fluence. The dark areas represent the strain fields associated to extended defects with a diameter close to 6 nm for the largest ones. These extended defects have neutral charge and show deep energy levels [18]. The point defects are shallow ionized defects [19] with an activation energy value close to the one of the EL-2 like defect introduced by the low-temperature growth technique. All theses defects act as trap and recombination centers for free carriers thus reducing the carrier

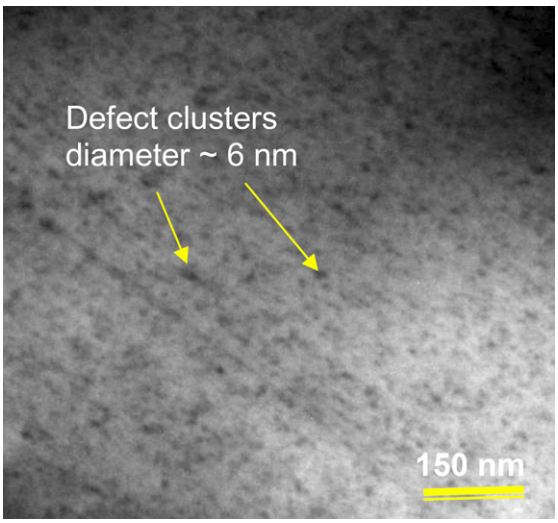

Fig. 1. 002 dark field image of $In_{0.53}Ga_{0.47}As$ layers after irradiation with Au^+ at very high irradiation dose (1×10^{12} cm^{-2}). The dark areas represent the strain fields associated to extended defects with a typical diameter closed to 6 nm for the largest ones.

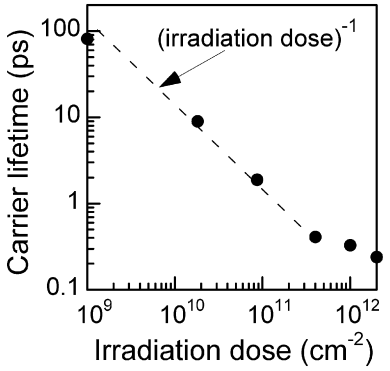

Fig. 2. Carrier lifetime in heavy-ion-irradiated $In_{0.53}Ga_{0.47}As$ layer as a function of the irradiation dose, extracted from time-resolved differential transmittance.

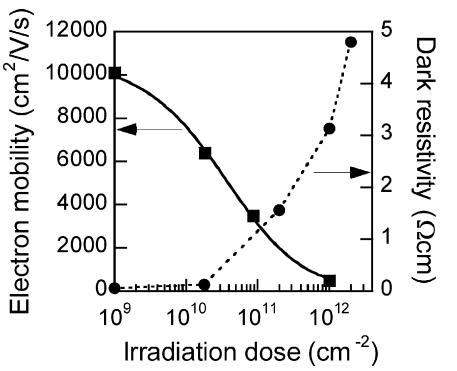

Fig. 3. Hall electron mobility (square) and dark resistivity (circle) in heavy-ion-irradiated $In_{0.53}Ga_{0.47}As$ material versus irradiation dose. The solid line represents the fit by a model of electron scattering on neutral centers (extended defects) and ionized centers (point defects).

Table 1
Summary of reported results for ultrafast photoconductive antennas based on $In_{0.53}Ga_{0.47}As$ material

Material	Carrier lifetime (ps)	Dark resistivity (Ω cm)	Reported applications
LTG $In_{0.53}Ga_{0.47}As$	∼2–3	200	Detection of pulsed terahertz radiation from photoconductive antenna
Be doped $In_{0.53}Ga_{0.47}As$:ErAs	0.3	500	Generation of continuous wave from photomixer
Fe implanted $In_{0.53}Ga_{0.47}As$	0.3	few hundreds	Emission and detection of terahertz pulsed radiation from photoconductive antenna
Heavy-ion-irradiated $In_{0.53}Ga_{0.47}As$	0.3	∼5	Emission and detection of terahertz pulsed radiation from photoconductive antenna

lifetime. The carrier lifetime in heavy-ion-irradiated $In_{0.53}Ga_{0.47}As$ layers have been extracted from all-optical pump-probe scheme experiments at 1.55 μm central wavelength. Fig. 2 reports the carrier lifetime versus the irradiation dose for doses varying from 1×10^{10} to 4×10^{12} cm^{-2}. The carrier lifetime is found to be inversely proportional to the irradiation dose according to the Schockley–Read–Hall model. The shortest carrier lifetime is less than 300 fs. Moreover, a remarkable characteristic of the ion irradiation method is that the carrier lifetime is easily adjustable through the irradiation dose from thousands picosecond to sub-picosecond values [20]. Fig. 3 shows that the Hall electron mobility is reduced with the increase of the irradiation dose, and this evolution is well fitted by a model of electron mobility governed by scattering on neutral centers (extended defects) and ionized centers (point defects). The residual carrier density is quasi-invariant whatever the irradiation dose. As a consequence, the semi-insulating properties of the intrinsic $In_{0.53}Ga_{0.47}As$ material are not significantly modified after heavy-ion irradiation. Thereby, the dark resistivity increase with the increase of the irradiation dose observed in Fig. 3 is essentially due to the electron mobility degradation. Finally, annealing measurements have shown that the specific spatial distribution of defects in clusters is particularly robust against thermal annealing.

The optical and electrical properties of heavy-ion-irradiated $In_{0.53}Ga_{0.47}As$ material, reported in Table 1, indicate that this is a material of choice for the development of terahertz emitters and receivers gated with femtosecond optical pulses at 1550 nm wavelength.

4. Terahertz emission and detection using femtosecond optical pulses at 1.55 μm wavelength

4.1. Device fabrication

Photoconductive antennas based on heavy-ion-irradiated $In_{0.53}Ga_{0.47}As$ material have been made. Undoped 1-μm-thick n-type $In_{0.53}Ga_{0.47}As$ layers were epitaxially grown by gas-source MBE on semi-insulating InP:Fe substrates. A mesa etching process was used to define $In_{0.53}Ga_{0.47}As$ absorbing area of 82×14 μm^2 and 7×14 μm^2 on the

InP substrate for emitters and detectors, respectively. The layers were then irradiated by 11 MeV heavy ions (Br^+) at irradiation doses from 1×10^{10} cm^{-2} to 1×10^{12} cm^{-2}. Furthermore, a thin cap layer of optical transparent silicon nitride was grown to protect the device from oxidation and to provide an antireflection coating. The electrode patterns were fabricated by metal evaporation and a conventional lift-off photolithographic technique. Then, the antenna structure is located at the center of a 20-mm-long coplanar transmission line consisting of simple coplanar striplines patterned onto the InP substrate. The latter are made of two 5-μm-wide, 0.5-μm-thick Ti/Au strips separated by 80 μm and 30 μm for emitters and detectors, respectively. For the detector, a gap of 5 μm between the contacts is added.

The dark current-voltage characteristic of the un-irradiated device is nonlinear since the current, limited by the inverse contact, is due to the thermoionic emission of electrons above the Schottky barrier. With the increase of the irradiation dose, the dark current-voltage characteristic tends to be linear at low voltage. The transport regime is therefore governed by ohmic conduction in the $In_{0.53}Ga_{0.47}As$ layer rather than by the Schottky contacts. Above ∼25 V, the current begins to increase quadratically with applied voltage due to space-charge-limited current. Such nonlinear characteristic is partly responsible for the field-enhanced terahertz response observed when the exciting laser pulse is in close proximity to the anode of the photoconductive emitter [21].

4.2. Time domain experiments

We have developed a time-domain terahertz spectroscopy set up based on Er:fiber laser at 1.55 μm wavelength and on heavy ion-irradiated $In_{0.53}Ga_{0.47}As$ photoconductive antennas as emitter and as detector. The passively mode-locked fiber laser delivered 250 fs optical pulse with central wavelength at 1550 nm and a repetition rate of 14.3 MHz. The optical pulse is divided by a beam splitter into an excitation pulse incident on the emitter, and into a trigger pulse incident on the detector. The optical excitation beam was focused on the emitter with a spot size of about 10 μm, near the anode of the antennas. The optical trigger beam was focused on the detector with a spot size of about 5 μm. High-resistivity Si hyperhemispherical substrate lenses, with a 10 mm diameter, were attached back to the emitter and the receiver antennas. The intensity of the terahertz radiation was modulated using a mechanical chopper. The detector was placed 5 cm away from the emitter. The current induced by the probe beam and the terahertz radiation in the detector is amplified and processed with a lock-in digital amplifier. Note that the InP substrate does not absorb the 0.8 eV photons (since the laser fluences are relatively low [22]) and its contribution on the terahertz emission and detection is negligible.

4.2.1. Terahertz pulsed generation and detection

The signal waveform emitted and detected by heavy-ion-irradiated $In_{0.53}Ga_{0.47}As$ photoconductive antennas with 0.3 ps lifetime is shown in Fig. 4. The average power of the both optical beams is 3 mW. In the approximation of the dipole antennas, the emitted transient field waveforms in the far field approximation is related to the temporal derivative

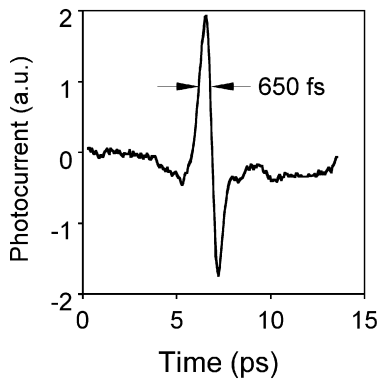

Fig. 4. Time resolved waveform of terahertz radiation from Br^+-irradiated $In_{0.53}Ga_{0.47}As$ photoconductive antenna and detected by Br^+-irradiated $In_{0.53}Ga_{0.47}As$ photoconductive antenna.

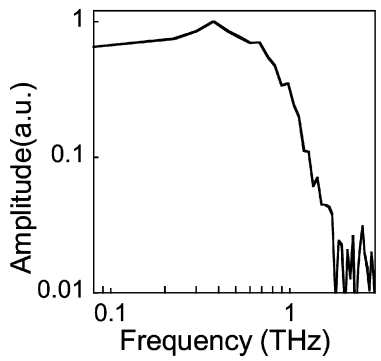

Fig. 5. Normalized spectra of the terahertz waveforms radiated from Br^+-irradiated $In_{0.53}Ga_{0.47}As$ photoconductive antenna and detected by Br^+-irradiated $In_{0.53}Ga_{0.47}As$ photoconductive antenna.

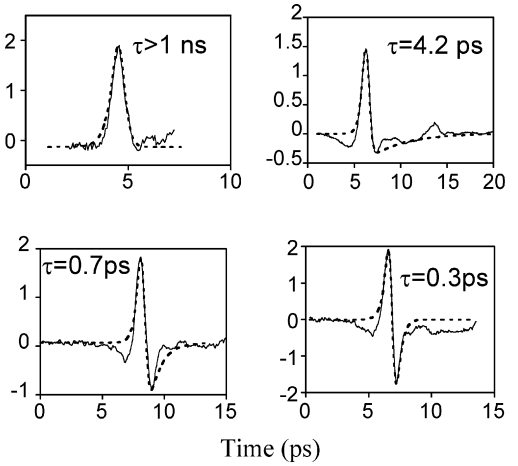

Fig. 6. Terahertz radiation waveforms from Br^+-irradiated $In_{0.53}Ga_{0.47}As$ emitters. The solid lines represent the measured waveforms and the dashed lines the calculated waveforms. The carrier lifetime reported on each graph is the carrier lifetime extracted from optical pump-probe differential transmission measurements.

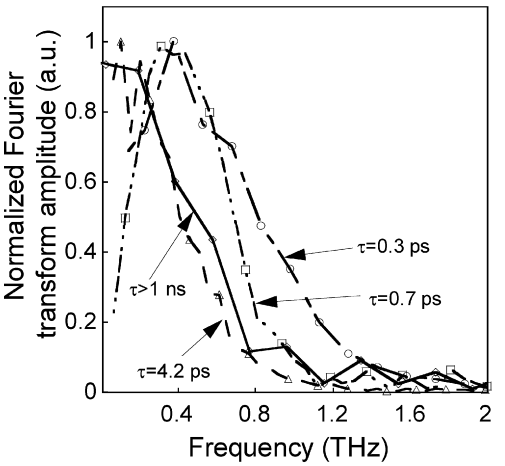

Fig. 7. Normalized spectra of the terahertz waveforms for emitters with different carrier lifetime.

of the transient current: $E_{\mathrm{THz}} \propto \partial J(t)/\partial t$. The main positive peak of the waveform, which shows a full-width-at-half-maximum (FWHM) of 650 fs, results from the ultrafast rise of the surge current by the photocarrier injection and the subsequent carrier acceleration under the bias field of the photoconductive antennas. The main positive peak is followed by a negative peak, attributed to the decay of the current. The negative peak, with relative amplitude of 90% of the main peak, is attributed to the fast current decay governed by carrier trapping in sub-picosecond time scale. Fig. 5 displays the radiation power spectrum calculated from the fast Fourier transform (FFT) of the waveform in Fig. 4. The spectrum is centered at 376 GHz and extends beyond 1.5 THz with ∼30 dB dynamic below 0.7 THz. The performances of this time-domain spectroscopy set up based on Er:fiber laser are relatively good when one considers the low average optical powers incident on the emitter and on the detector, due to the limited total optical power delivered by this fiber laser source.

4.2.2. Carrier lifetime influence on emitted terahertz radiation characteristics

The material investigation reported in Section 2 has revealed that the carrier lifetime in semiconductor layers can be reduced in a controlled way by the ion irradiation technique. This feature allows the study of how the carrier lifetime impacts on the emitted terahertz signal characteristics. Such an investigation turns out to be crucial for applications as carrier lifetime strongly influences the spectral distribution and the radiated power emitted by photoconductive antennas [23,24]. In this section, we present a detailed study of the effect of the carrier lifetime on the terahertz radiation characteristics emitted by Br^+-irradiated $In_{0.53}Ga_{0.47}As$ photoconductive antennas; we investigated four $In_{0.53}Ga_{0.47}As$ emitters with different carrier lifetimes, namely >1 ns, 4.2 ps, 0.7 ps and 0.3 ps. The carrier lifetime in the detector was 0.3 ps for all measurements. The signal waveforms emitted from the four photoconductive antennas are shown in Fig. 6. These results are obtained using an applied bias voltage of 7 V for the long carrier lifetime sample and bias voltages higher than 15 V for samples with picosecond carrier lifetimes.

The waveform emitted by the un-irradiated photoconductive antenna is unipolar whereas the waveforms emitted by the ion-irradiated samples are bipolar and are depicted by a main positive peak followed by a negative peak. As the carrier lifetime decrease, the negative peak controlled by the picosecond carrier lifetime is more intense and happens earlier. The origin of the negative peak observed to occur before the main positive peak is attributed to the pulse reshaping effect due to the frequency dependent THz beam focus on the detector antenna [25]. Small oscillations are observed after the negative peak and may be the result of resonance effects in the emitting antenna and of plasma type oscillations. The transition from unipolar radiation to almost nearly symmetrical bipolar transition with the decrease of the carrier lifetime are well described by the analytical model based on classical charge transport and dipole radiation given by Duvillaret et al. [26]. This model assumes among others that a single exponential decay law governs the

free-carrier relaxation in both emitter and detector. When considering the broadening of the terahertz pulse in the Fe:InP substrates of the two antennas, the detected photocurrent is expressed by:

$$
\begin{aligned}
j_{\mathrm{rec}}(t) \propto \int \mathrm{d}t' \, (\tau_{\mathrm{em}} + \tau_{\mathrm{rec}}) \exp\left(\frac{\tilde{\tau}_{\mathrm{las}}^2}{2\tilde{\tau}_{\mathrm{em}}^2} - \frac{t}{\tilde{\tau}_{\mathrm{em}}}\right) \operatorname{erfc}\left(\frac{\tilde{\tau}_{\mathrm{las}}^2 - t\tilde{\tau}_{\mathrm{em}}}{\sqrt{2}\tilde{\tau}_{\mathrm{em}}\tilde{\tau}_{\mathrm{las}}}\right) \\
+ (\tau_{\mathrm{em}} - \tilde{\tau}_{\mathrm{em}}) \exp\left(\frac{\tilde{\tau}_{\mathrm{las}}^2}{2\tau_{\mathrm{rec}}^2} - \frac{t}{\tau_{\mathrm{rec}}}\right) \operatorname{erfc}\left(\frac{\tilde{\tau}_{\mathrm{las}}^2 + t\tau_{\mathrm{rec}}}{\sqrt{2}\tau_{\mathrm{rec}}\tilde{\tau}_{\mathrm{las}}}\right) \\
- (\tau_{\mathrm{rec}} + \tilde{\tau}_{\mathrm{em}}) \exp\left(\frac{\tilde{\tau}_{\mathrm{las}}^2}{2\tau_{\mathrm{em}}^2} - \frac{t}{\tau_{\mathrm{em}}}\right) \operatorname{erfc}\left(\frac{\tilde{\tau}_{\mathrm{las}}^2 + t\tau_{\mathrm{em}}}{\sqrt{2}\tau_{\mathrm{em}}\tilde{\tau}_{\mathrm{las}}}\right) \exp\left(-(t-t')^2/2\Delta t\right)
\end{aligned}
$$

with $1/\tilde{\tau}_{\mathrm{em}} = 1/\tau_{\mathrm{em}} + 1/\delta\tau_{\mathrm{em}}$ and $\tau_{\mathrm{em}}, \tau_{\mathrm{rec}}, \tau_{\mathrm{las}}, \delta\tau_{\mathrm{em}}$ are the carrier lifetime in the emitter, the carrier lifetime in the detector, the laser pulse duration and the carrier collision time respectively and Δt is the temporal broadening due to the dispersion in the substrates. The dotted lines in Fig. 6 are the waveforms calculated with $\tau_{\mathrm{rec}} = 330$ fs, $\tau_{\mathrm{las}} = 250$ fs, $\delta\tau_{\mathrm{em}} = 180$ fs [27] and $\Delta t = \Delta n l/c \approx 200$ fs since we measured, by time domain terahertz spectroscopy, the maximum variation of refraction index Δn in Fe:InP in the considered frequency range to be approximately 0.09. We did not compare the absolute amplitudes since they are sensitively dependent on the critical positioning of the Si lens on the detector. The best fits is obtained for carrier lifetime values of 0.3 ps, 0.9 ps, 3.9 ps which are very close to the values measured by optical pump-probe differential transmittance experiments.

Fig. 7 displays the normalized Fourier transform amplitude spectra of the temporal waveforms. Just as the temporal behaviour depends on the carrier lifetime in the emitter, the spectral peaks depend on these carrier lifetimes, being shifted to higher frequency when decreasing the carrier lifetime. The maximum of the spectrum is shifted from a frequency inferior to 0.05 THz for the un-irradiated $In_{0.53}Ga_{0.47}As$ photoconductive antenna to a frequency of 0.38 THz for the most irradiated $In_{0.53}Ga_{0.47}As$ photoconductive antenna (1×10^{12} cm^{-2}). Improvement in the spectral bandwidth of the emitted terahertz radiation is then observed with the decrease of the carrier lifetime on the emitter.

4.3. Average radiated power

A point of prime importance is to know weather the increase of the spectral bandwidth with the decrease of the carrier lifetime occurs at the cost of a reduced emission power. In the previous experiments, the comparison of the emitted radiation amplitudes by the different photoconductive antennas was prevented by the critical positioning of the Si lens on the detector due to its extremely small area (5 μm). To ensure an accurate comparison, we have used a 3 mm-diameter silicon diamond composite bolometer as detector. The bolometer, with an optical sensitivity of 4.6×10^5 V/W, was located just in front of the Si lens placed on the back of the photoconductive antenna emitters. The emitters were excited by 200 fs optical pulses with 1550 nm central wavelength and with 80 MHz repetition rate produced by an optical parametric oscillator pumped by a mode-locked Ti:sapphire laser. The mode-locked Ti:sapphire laser delivered 200 fs optical pulses with 780 nm central wavelength.

At the same bias voltage, the radiated terahertz power was found to decrease with the increase of the irradiation dose. This drop of the radiated power is attributed to the reduction of both the photo-carrier mobility and the carrier lifetime with the increase of the irradiation dose. Indeed, theoretical works have shown that the emitted terahertz power is lowered with the decrease of the carrier lifetime and the photo-carrier mobility [5]. Fig. 8 represents the absolute terahertz power, as a function of the incident laser power, emitted by $In_{0.53}Ga_{0.47}As$ photoconductive antennas operating at their maximum possible bias voltage. The maximum bias voltages, which remains below the electric breakdown and also below the threshold for thermal runaway, were 16 V, 28 V, 40 V and 60 V for the samples with carrier lifetimes of >1 ns, 4.2 ps, 0.7 ps and 0.3 ps respectively. The highest achieved power is delivered by photoconductive antennas having 0.7 ps carrier lifetime and is equal to 0.8 μW. Moreover, it can be seen in Fig. 8 that the emitted terahertz power increases with the increase of the irradiation dose until the lifetime is reduced down to 0.7 ps. This increase of the terahertz power is attributed to the increase of the maximum possible bias voltage since the terahertz power is proportional to the square of the applied electric field. For the photoconductive antenna with 0.3 ps carrier lifetime, the decrease of the radiated power is attributed to carrier recombination that occurred before the end of the optical pulse as the carrier lifetime is comparable to the pulse duration.

The performance of these ion-irradiated $In_{0.53}Ga_{0.47}As$ photoconductive antennas have been directly compared to those of a typical LTG GaAs photoconductive antenna by measuring the delivered terahertz power in the same

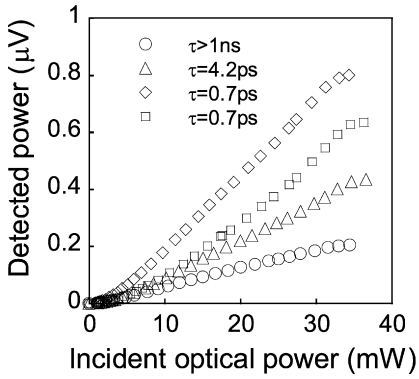

Fig. 8. Detected terahertz power as a function of the average laser power driving the emitter for photoconductive antennas with different carrier lifetimes. The solid curve is the theoretical curve fitted to the data based on a saturation model.

experimental set up and with the same calibrated bolometer. The LTG GaAs device was a similar 80-μm-wide coplanar stripline antenna deposited onto LTG GaAs having a carrier lifetime of ∼1 ps. The power delivered by the LTG GaAs photoconductive antenna biased at 60 V and excited by an optical beam with a 36 mW average optical power at 780 nm central wavelength was 0.47 μW, in agreement with the measured powers reported by other group [28]. The terahertz powers emitted by ion-irradiated $In_{0.53}Ga_{0.47}As$ photoconductive antennas excited by 1550 nm wavelength optical pulses, which reached a maximum value of 0.8 μW, are then comparable with or greater than that emitted by LTG-GaAs photoconductive antennas excited by 780 nm wavelength optical pulses.

4.4. Saturation effects

For all samples, the radiated power increases quadratically at low incident optical powers and saturates at higher incident optical powers as observed in Fig. 8. This saturation is attributed to the screening of the applied bias field by the radiation field and the space-charge field, which contribute to the collapse of the total electric field acting on the carriers at high carrier density. For small optical size excitation (small-aperture emitters), models based on the Monte Carlo method have shown that the space charge induced by separating carriers is the dominant contribution to the screening of the applied electric field [29,30]. From a simple model that considers the difference of mobilities of electrons and holes and its consequence on the local electric field, the average terahertz power can be expressed [31] by $P_{\mathrm{THz}} \propto (F_{\mathrm{laser}}/F_0 + F_{\mathrm{laser}})^2$ with F_0 defined by $\varepsilon h\nu/(q\alpha(1 - \mathrm{e}^{-\alpha l})\mu\tau_{\mathrm{las}}$. The solid lines in Fig. 8 represent the fit of the experimental data. Assuming that the only irradiation fluence-dependent parameter of F_0 is the photoexcited carrier mobility, a photoexcited carrier mobility ratio of 3 between the un-irradiated sample and the sample with 0.3 ps carrier lifetime was estimated. This ratio is clearly lower than the Hall carrier mobility ratio of 23 measured between these two samples. The difference is explained because Hall mobility is the low electrical field mobility obtained with a carriers in low density (10^{15} cm^{-3}), whereas the mobility involved in these measurements results from higher electrical field and from a high concentration of photocreated carriers (few 10^{17} cm^{-3}). The irradiation process affects much more the electron Hall mobility due to the defect scattering than the effective mobility of photoexcited carriers in the early stage after their creation.

Fig. 9 shows the radiated power as a function of the carrier lifetime in $In_{0.53}Ga_{0.47}As$ photoconductive antennas, computed for different frequencies from time domain measurements with Bolometer detector normalization. The decrease of the carrier lifetime on the emitter improves the bandwidth and the average power of the emitted terahertz radiation, thanks to the increase of the maximum possible bias voltage with the increase of the ion irradiation dose. These results have important practical implications for terahertz emitter design: the carrier lifetime in the emitter can be adjusted to reach a specific terahertz spectral range.

5. Towards short wavelength

To go further in the investigation of ion-irradiated $In_{0.53}Ga_{0.47}As$ photoconductive antennas, we have studied a spectral extension of the optical excitation, in particular at 800 nm wavelength. This investigation was motivated by the

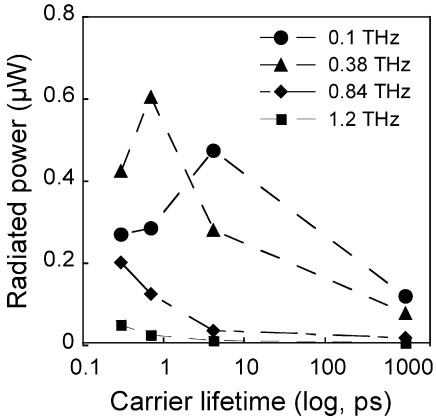

Fig. 9. Emitted terahertz power as a function of the carrier lifetime at 0.1 THz (circle), 0.38 THz (triangle), 0.84 THz (diamond) and 1.2 THz (square) computed from time domain measurements with bolometer detector normalization.

perspective to develop optical pump-terahertz probe experiments using ion-irradiated $In_{0.53}Ga_{0.47}As$ photoconductive antennas as emitter and detector. Indeed, there is a strong interest to have terahertz sources which can be driven with optical commands in a relatively large panel of wavelengths, as a specific wavelength excitation is required depending on the object under study. Under optical excitation at 800 nm central wavelength, photoexcited carriers in $In_{0.53}Ga_{0.47}As$ are transferred in the L satellite valleys in contrast to standard optical excitation at 1550 nm wavelength for which photoexcited carriers remain in Γ valley.

The time-domain terahertz spectroscopy set up used for this experiment is similar to that reported in Section 4.2, except that the optical source is a mode-locked Ti–sapphire laser that generates 800 nm center wavelength pulses, at a repetition rate of 76 MHz and with a 100 fs full width at half-maximum duration. Two photoconductive antennas, with similar antenna design, and made from 1×10^{12} cm^{-2} Br^+-irradiated $In_{0.53}Ga_{0.47}As$ with a carrier lifetime of $\sim$0.3 ps and from LTG GaAs with a carrier lifetime of $\sim$1 ps were fabricated.

The temporal terahertz waveforms emitted by the ion-irradiated $In_{0.53}Ga_{0.47}As$ and the LTG GaAs photoconductive antennas excited by femtosecond optical pulse at 800 nm central wavelength are shown in Fig. 10. An external voltage source of 7 V was applied to $In_{0.53}Ga_{0.47}As$ photoconductive antennas and the average optical excitation power was 28 mW. To ensure a comparable absorbed power, the average optical excitation power incident on the LTG GaAs photoconductive antenna was 40 mW. The voltage across LTG GaAs photoconductive antenna was 60 V. A LTG GaAs dipole antenna was used for the detection. The positive peaks of the two waveforms show a full width at half-maximum of 650 fs. The detected current peak associated with the waveforms radiated by the $In_{0.53}Ga_{0.47}As$ and the LTG GaAs PA are respectively 0.73 nA and 1 nA. In the $In_{0.53}Ga_{0.47}As$ material, alterations in the carrier dynamic transport and in the relaxation delay are expected since the photocarriers have excess energy. Nevertheless, the temporal characteristics are not degraded compared to LTG GaAs ones. Moreover, the irradiated-$In_{0.53}Ga_{0.47}As$ shows a remarkable conversion efficiency since its applied bias field is around 9 times lower than for LTG GaAs. Fig. 10 displays the fast Fourier transform amplitude spectra of these temporal waveforms. For both emissions, the frequency range is 0.1 to 2 THz with 50 dB dynamic below 0.7 THz, showing that $In_{0.53}Ga_{0.47}As$ emission spectrum is comparable to that of LTG GaAs photoconductive emitter [32].

The temporal terahertz waveform detected by the 1×10^{12} cm^{-2} irradiated-InGaAs photoconductive antennas is presented in Fig. 11. 49 mW optical power is used to gate the terahertz signal. The terahertz radiation is emitted by a LTG GaAs dipole antenna biased at 30 V and excited by 30 mW optical excitation. The positive peak current of the detected waveform shows a full width at half-maximum of 860 fs. The amplitude is 5.3 nA. The insert shows the fast Fourier transforms of the terahertz waveform detected by the $In_{0.53}Ga_{0.47}As$ irradiated sample. As for emission, the frequency range is 0.1 to 2 THz with 50 dB dynamic. The performances in detection are also closed to those obtained with LTG GaAs in spite of the lower resistivity of the $In_{0.53}Ga_{0.47}As$ photoconductive antenna.

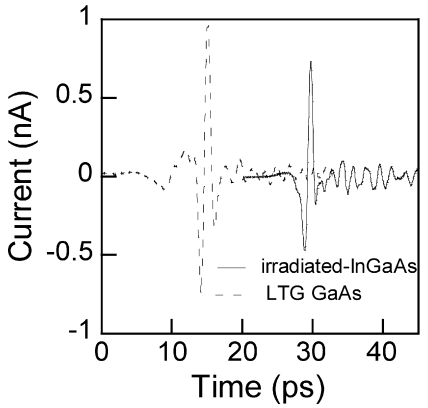

Fig. 10. Temporal terahertz radiation waveforms emitted from ion-irradiated $In_{0.53}Ga_{0.47}As$ and LTG GaAs strip lines and detected by a LTG GaAs dipole antenna.

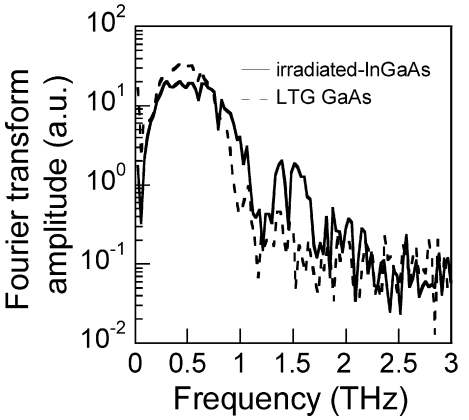

Fig. 11. Fourier-transformed amplitude spectrum of the temporal waveforms emitted from ion-irradiated $In_{0.53}Ga_{0.47}As$ and LTG GaAs strip lines.

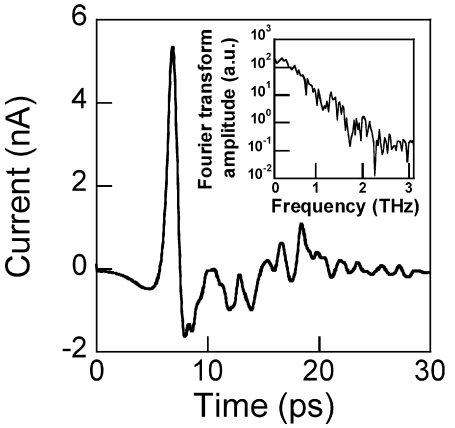

Fig. 12. Temporal terahertz radiation waveform detected by ion-irradiated $In_{0.53}Ga_{0.47}As$ strip lines. A LTG GaAs dipole antenna is used for emission. The insert is the Fourier-transform amplitude spectrum.

6. Concluding remarks

Heavy-ion-irradiated $In_{0.53}Ga_{0.47}As$ photoconductive antennas gated with 1.55 μm wavelength femtosecond laser pulses are good candidates as emitter and receiver of broadband terahertz radiation. The average radiated power, which reached 0.8 μW, is comparable with or greater than that emitted by similar low temperature grown GaAs photoconductive antennas excited by 0.78 μm wavelength optical pulses. Enhancement of the radiated terahertz power should be achieved by, in particular, the optimization of the antenna design [33]. The integration of such devices in a time domain terahertz spectroscopy system will take advantage of the superior laser and fiber technology available at telecommunication wavelengths and will enable the development of compact, low cost and more stable systems.

Acknowledgements

The authors would like to thank S. Henry and C. Boukari and H. Bernas from CSNSM in Orsay for ion irradiation, K. Blary and J.F. Lampin from IEMN for device technological fabrication, P. Mounaix and M. Tondusson from CPMOH for experiments at 800 nm wavelength, G. Patriarche from LPN for transmission electron microscopy ex-

periments and G. Fishman and N. Zerounian from IEF for fruitful discussions. This work has been carried out in the framework of the French RTB network.

References

[1] A.C. Warren, N. Katzenellenbogen, D. Grischkowsky, J.M. Woodall, M.R. Melloch, N. Otsuka, Appl. Phys. Lett. 58 (1991) 1512.
[2] Y.C. Shen, P.C. Upadhya, E.H. Linfield, H.E. Davies, A.G. Davies, Appl. Phys. Lett. 83 (2003) 3117.
[3] S. Kono, M. Tani, K. Sakai, Appl. Phys. Lett. 79 (2001) 898.
[4] Y.C. Shen, P.C. Upadhya, E.H. Linfield, H.E. Davies, A.G. Davies, I.S. Gregory, C. Baker, W.R. Tribe, M.J. Evans, Appl. Phys. Lett. 85 (2004) 164.
[5] J. Lloyd-Hughes, E. Castro-Camus, M.B. Johnston, Solid State Commun. 136 (2005) 595–599.
[6] B.C. Tousley, S.M. Mehta, A.I. Lobad, P.J. Rodney, P.M. Fauchet, P. Cooke, J. Electron. Matter 22 (1993) 1477.
[7] H. Kunzel, J. Bottcher, R. Gibis, G. Urmann, Appl. Phys. Lett. 61 (1992) 1347.
[8] P.W. Joudawlkis, D.T. McInTurff, S.E. Ralph, Appl. Phys. Lett. 69 (1996) 4032.
[9] A. Takazato, M. Kamakura, T. Matsui, J. Kitagawa, Y. Kadoya, Appl. Phys. Lett. 90 (2007) 101119.
[10] D.C. Driscoll, M. Hanson, C. Kadow, A.C. Gossard, J. Vacuum Sci. Technol. B: Microelectron. Nanometer Struct. 19 (2001) 1631.
[11] D.C. Driscoll, M.P. Hanson, A.C. Gossard, E.R. Brown, Appl. Phys. Lett. 86 (2005) 051908.
[12] M. Sukhotin, E.R. Brown, A.C. Gossard, D. Driscoll, M. Hanson, P. Maker, R. Muller, Appl. Phys. Lett. 82 (2003) 3116.
[13] C. Carmody, H.H. Tan, C. Jagadish, A. Garder, S. Marcinkevicius, Appl. Phys. Lett. 82 (2003) 3913.
[14] M. Suzuki, M. Tonouchi, Appl. Phys. Lett. 86 (2005) 1104.
[15] M. Suzuki, M. Tonouchi, Appl. Phys. Lett. 86 (2005) 163504.
[16] J.F. Ziegler, J.P. Biersack, U. Littmark, The Stopping and Range of Range of Ions in Solids, Pergamon, New York, USA, 1985.
[17] L. Joulaud, J. Mangeney, J.M. Lourtioz, P. Crozat, G. Patriarche, Appl. Phys. Lett. 82 (2003) 856.
[18] L. Joulaud, J. Mangeney, N. Chimot, P. Crozat, G. Fishman, J.C. Bourgoin, J. Appl. Phys. 97 (2005) 63515.
[19] J. Mangeney, N. Stelmakh, F. Aniel, P. Boucaud, J.-M. Lourtioz, Appl. Phys. Lett. 80 (2002) 4711.
[20] J. Mangeney, L. Joulaud, J. Decobert, J.M. Lourtioz, J.L. Perrossier, S. Cabaret, P. Crozat, Electron. Lett. 39 (2003) 681.
[21] S.E. Ralph, D. Grischkowsky, Appl. Phys. Lett. 59 (1991) 1972.
[22] D. Vignaud, J.F. Lampin, F. Mollot, Appl. Phys. Lett. 85 (2004) 239–241.
[23] B. Salem, D. Morris, V. Aimez, J. Beauvais, D. Houde, Semicond. Sci. Technol. 21 (2006) 283–286.
[24] S.G. Park, A.M. Weiner, M.R. Melloch, C.W. Siders, J.L.W. Siders, A.J. Taylor, IEEE J. Quantum Electron. 35 (1999) 1257.
[25] P.U. Jepsen, R.H. Jacobsen, S.R. Keiding, J. Opt. Soc. Am. B 13 (1996) 2424.
[26] L. Duvillaret, F. Garet, J.-F. Roux, J.-L. Coutaz, IEEE J. Selected Topics in Quantum Electron. 7 (2001) 615.
[27] This value is consistent with the values given by P.Y. Yu, M. Cardona, Fundamentals of Semiconductors, second ed., Springer, 1999, p. 290.
[28] M. Tani, S. Matsura, K. Sakai, S. Nakashima, Appl. Opt. 36 (1997) 7853.
[29] E. Castro-Camus, J. Lloyd-Hughes, M.B. Johnston, Phys. Rev. B 71 (2005) 195301.
[30] D.S. Kim, D.S. Citrin, Appl. Phys. Lett. 88 (2006) 161117.
[31] J. Mangeney, N. Chimot, L. Meignien, N. Zerounian, P. Crozat, K. Blary, J.F. Lampin, P. Mounaix, Opt. Express 15 (2007) 8943.
[32] N. Chimot, J. Mangeney, P. Mounaix, M. Tondusson, K. Blary, J.F. Lampin, Appl. Phys. Lett. 89 (2006) 083519.
[33] Z.D. Taylor, E.R. Brown, J.E. Bjarnason, M.P. Hanson, A.C. Gossard, Opt. Lett. 31 (2006) 1729.